Supporting Material

for

Unfolding of a small protein proceeds *via* dry and wet globules and a solvated transition state

Saswata Sankar Sarkar[1], Jayant B. Udgaonkar[2*], G. Krishnamoorthy[1*]

[1] Department of Chemical Sciences, Tata Institute of Fundamental Research, Mumbai 400005, India,

[2] National Centre for Biological Sciences, Tata Institute of Fundamental Research, Bangalore 560065, India

* To whom correspondence should be addressed.

Telephone: 91-80-23666150, E-mail: jayant@ncbs.res.in

Telephone: 91-22-22782301, E-mail: gk@tifr.res.in

Supporting Material:

Supporting Material Text:

The stabilities and unfolding rates of the unlabeled and labeled proteins are the same

In this study, all the time-resolved fluorescence measurements, fluorescence intensity measurements, and the CD measurements were carried out with the unlabeled Cys82 variant of barstar. FRET measurements were carried out with TNB-labeled Cys82 (Cys82-TNB), as well as with the TNB-labled Cys25 variant (Cys25-TNB). It was shown previously that unlabeled and TNB-labeled Cys82, as well as unlabeled and TNB-labeled Cys25, all have the same stabilities (1) as well as the same folding rates (2). It was also important to show that all four proteins unfold with similar kinetics. Fig. S1 shows the unfolding kinetics of Cys82, Cys82-TNB, Cys25 and Cys25-TNB, monitored by far-UV CD. It is seen that all four proteins unfold with similar exponential kinetics with an apparent rate of $0.32 \pm 0.04\ s^{-1}$ (Fig. S1). It should also be noted that FRET monitored slow rate of Cys25-TNB and the FRET-monitored rate of Cys82-TNB are very similar in value each other and to the CD monitored rates, and that the kinetics of Cys25-TNB are different only in that an additional 10-fold faster phase is seen.

FRET-monitored unfolding

FRET measurements were carried out by measurement of the increase in fluorescence intensity of the labeled proteins Cys25-TNB and Cys82-TNB at 387 nm. At this wavelength the quantum yield of fluorescence of W53 is similar in the N and U states of the unlabeled proteins Cys25 and Cys82, and there is no fast component in the change in fluorescence during the unfolding of the unlabeled proteins (data not shown), as seen in the case of FRET in Cys25-TNB. In the comparison of FRET changes during the unfolding of the two labeled proteins, it is important to remember that the donor W53 is the same in the two proteins, and its quantum yield and rotational freedom will change in an identical manner during the unfolding of both proteins.

Supporting Material - Materials and Methods:

Proteins, chemicals, buffers and TNB labeling

The mass of purified protein was checked by ESI mass spectrometry. The time-resolved fluorescence measurements, fluorescence intensity measurements, and CD measurements were all carried out on the Cys82 mutant form of barstar (1). FRET measurements are carried out on Cys82 as well as on the Cys25 mutant variant. All the chemicals used were of the highest purity grade available from Sigma Aldrich, Inc. Native buffer containing 20 mM Tris and 250 μM EDTA at pH 8.0 was used for experiments. Unfolding buffer contained denaturant in addition to native buffer. For TNB labeling, unfolded protein in 6 M GdHCl unfolding buffer at pH 8.5 was incubated with a 100-fold excess of 5,5' Dithiobis (2-nitrobenzoic acid) (DTNB) in same buffer for an hour. Labeled protein was purified using a PD10 column (GE Health Care Life Sciences).

Kinetic unfolding experiments monitored by steady state fluorescence and CD

All the kinetic experiments were performed using the SFM400 stopped-flow mixing module from Biologic, as described earlier (4). A FC-15 cuvette with a pathlength of 1.5 mm was used for fluorescence and far-UV CD measurements, and a TC100/10 cuvette with a 1 cm pathlength was used for near-UV CD measurements. N_2 was purged around the cuvette throughout the experiment to avoid condensation of moisture on its wall. In the stopped-flow

module, the unfolding kinetic reaction was initiated by mixing native protein with unfolding buffer and native buffer at different mixing ratios to reach the final urea concentration of 5.0 to 6.5 M. For fluorescence measurements, an MOS450 optical system was coupled to stopped-flow to monitor steady state fluorescence. Tryptophan was excited at 295 nm and emission was observed at 350 nm and 387 nm using separate band pass filters for fluorescence intensity measurements of unlabeled and labeled protein, respectively. However, a monochromator was attached to the system to collect kinetic unfolding traces at different wavelengths for the spectra measurement. The concentrations of protein used were 5 and 15 μM for unlabeled and labeled protein, respectively.

The stopped-flow was coupled to a JASCO J-815 spectropolarimeter for CD monitored kinetic measurements. The CD signal was monitored at 222 nm and 270 nm for far- and near-UV CD measurements. Four kinetic traces were averaged for far-UV CD measurements, whereas nine kinetic traces were averaged for near-UV CD measurements to improve the S/N ratio of the data. The concentrations of protein used were 25 μM and 80-90 μM for far-UV CD and near-UV CD measurements, respectively.

Time-resolved fluorescence measurements

Fluorescence intensity decay traces during unfolding were collected using a double kinetic setup as described previously (5). 1 ps laser pulses of 885 nm at 80 MHz repetition rate from a Ti:Saphire laser, pumped by a Nd-YAG laser (Millenia X, Spectra Physics), were frequency tripled to 295 nm using a frequency doubler/tripler (GWU, Spectra Physics). The unfolding process was initiated in the stopped flow module by mixing the solutions of native barstar with unfolding buffer (6.6 M urea) in the ratio of 1:5 to get the final urea concentration of 5.5 M, and subsequent fluorescence decay traces were collected using the TCSPC instrument. Tryptophan was excited at 295 nm and the emission was observed at 350 nm using a combination of a monochromator and a 320 nm long-pass filter. Fluorescence decay traces at every 0.2 s of unfolding were captured. A L-format optical alignment (collection of fluorescence using a single PMT) was used for lifetime measurements, whereas a T-format alignment (collection of fluorescence using two different PMTs) was used for simultaneous collection of parallel and perpendicular polarized fluorescence light for anisotropy measurements. Fluorescence decays from 12 different stopped-flow kinetic experiments were added up to build the peak count in fluorescence anisotropy measurement for better S/N ratio. The peak counts were 3000 and 16000 for fluorescence quenching and anisotropy experiments, respectively. The instrument response function (IRF) was collected using a dilute colloidal suspension of dried non-dairy coffee whitener (5). Equilibrium measurements were done in the same TCSPC setup using an 1 ml cuvette instead of the stopped-flow cuvette. A protein concentration of 10 μM was used for all the measurements.

Analysis of time-resolved fluorescence data

For fluorescence lifetime measurements, the fluorescence decay curves collected at the magic angle (54.7˚) were analyzed by discrete analysis (3). The decay traces were deconvoluted with the IRF to obtain the intensity decay which was subsequently represented as a sum of 1-3 exponentials

$$I(t) = \sum_i \alpha_i \exp(-t/\tau_i) \qquad \text{(S1)}$$

where I(t) is the fluorescence intensity at time t and α_i is the amplitude of the i-th lifetime τ_i such that $\Sigma_i\alpha_i = 1$. Mean lifetime (τ_m) and intensity averaged lifetime (τ_a) were calculated using the equations: $\tau_m = \Sigma\alpha_i\tau_i$ and $\tau_a = (\Sigma\alpha_i\tau_i^2/ \Sigma\alpha_i\tau_i)$ respectively.

For the time-resolved fluorescence anisotropy measurements, the decays were analyzed by globally fitting $I_{\|}(t)$ and $I_{\perp}(t)$ as

$$I_{||}(t) = I(t)\,[1 + 2r(t)]/3 \quad \text{(S2)}$$

$$I_{\perp}(t) = I(t)\,[1 - r(t)]/3 \quad \text{(S3)}$$

where $I_{\|}(t)$ and $I_{\perp}(t)$ are the emission intensities collected at polarization directions parallel and perpendicular, respectively, to the polarization of the excitation beam.
The anisotropy, r (t) at any time t is given by,

$$r(t) = r_0\,[\beta \exp(-t/\varphi_F) + (1-\beta)]\exp(-t/\varphi_s) \quad \text{(S4)}$$

where r_0 is the initial anisotropy, φ_F is the fast correlation time, φ_S is the slow correlation time for overall tumbling of the macromolecule.

r(t) is, however, generally analyzed as the sum of two exponentials:

$$r(t) = r_0\,[\beta_{local} \exp(-t/\varphi_{local}) + \beta_{global} \exp(-t/\varphi_{global})] \quad \text{(S5)}$$

$$\text{with } \beta_{local} = \beta \;,\; \beta_{global} = 1-\beta \quad \text{(S6)}$$

$$\varphi_{global}^{-1} = \varphi_s^{-1}, \quad \varphi_{local}^{-1} = \varphi_s^{-1} + \varphi_F^{-1} \quad \text{(S7)}$$

Hence, the global correlation time, φ_{global}, can be equated with the slow correlation time, while the local correlation time, φ_{local}, is equal to the fast correlation time only when $\varphi_F << \varphi_S$.

The fluorescence anisotropy r(t) decay curve obtained at each time of unfolding was fit to eq S5 to obtain the value of β_{local} at each time of unfolding. For fitting the r(t) curves, the value of r_0 was constrained to a value of 0.2 ± 0.01. This was done because the value of r_0 for NATA in 75% glycerol was determined to be 0.2 ± 0.01 (data not shown), when the fluorescence excitation wavelength is 295 nm and emission wavelength is 350 nm, in agreement with previous work (5). It should be noted that the r_0 of indole is highly sensitive to the excitation wavelength due to the presence of overlapping excited states with orthogonal directions of the transition dipole (5).

Analysis of the fluorescence quenching data according to two-state and three-state models of unfolding

For a two-state model:

Model 1: $\mathrm{N} \xrightarrow{k} \mathrm{U}$

The unfolding kinetic traces obtained in the absence of acrylamide were fit to Eqs. S8 (fluorescence intensity data) or S9 (fluorescence lifetime data):

$$F(t) = F_{N,0.0}\exp(-kt) + F_{U,0.0}(1-\exp(-kt)) \quad \text{(S8)}$$

$$\tau(t) = \tau_{N,0.0}\exp(-kt) + \tau_{U,0.0}(1-\exp(-kt)) \quad \text{(S9)}$$

where F(t) represents the fluorescence intensity at time t during the unfolding, $F_{N,0.0}$ and $F_{U,0.0}$ are the relative fluorescence signals of the N and U states, respectively, k is the apparent rate of unfolding in the absence of both quencher and KCl for acrylamide quenching, and is the rate of the fast phase seen in the presence of 0.6 M KCl for KI quenching. For lifetime data, $\tau_{N,0.0}$ and $\tau_{U,0.0}$ are the mean lifetimes of N and U states respectively.

Similarly, kinetic traces in the presence of 0.6 M acylamide or KI were fit to Eqs. S10 (fluorescence intensity data) or S11 (fluorescence lifetime data):

$$F(t) = F_{N,0.6}\exp(-kt) + F_{U,0.6}(1-\exp(-kt)) \quad \text{(S10)}$$

$$\tau(t) = \tau_{N,0.6}\exp(-kt) + \tau_{U,0.6}(1-\exp(-kt)) \quad \text{(S11)}$$

$F_{N,0.6}$ and $F_{U,0.6}$ are the relative fluorescence signals of the N and U states, respectively, in the presence of 0.6 M quencher. $\tau_{N,0.6}$ and $\tau_{U,0.6}$ are the mean lifetimes in the N and U states, respectively, in the presence of 0.6 M quencher.

For two-state unfolding, the dependence of the value of k_q on the time of unfolding is described by Eq. S12:

$$k_q(t) = \frac{\left[\frac{\tau_{N,0.0}\exp(-kt) + \tau_{U,0.0}[1-\exp(-kt)]}{\tau_{N,0.6}\exp(-kt) + \tau_{U,0.6}[1-\exp(-kt)]} - 1\right]}{0.6\ \tau_{a,0.0}(t)} \quad \text{(S12)}$$

$\tau_{a,0.0}(t)$ is the intensity averaged lifetime in the absence of acrylamide at time t.

For three-state model, the kinetic scheme is shown below.

Model 2: $\mathrm{N} \xrightarrow{k_1} \mathrm{I} \xrightarrow{k_2} \mathrm{U}$

In the absence of quencher, the unfolding kinetic traces are described by Eqs. S13 (fluorescence intensity data) and S14 (fluorescence lifetime data):

$$F(t) = F_{N,0.0}\exp(-k_1 t) + F_{I,0.0}k_1\frac{[\exp((-k_1 t) - \exp(-k_2 t)]}{(k_2 - k_1)} + F_{U,0.0}\left(1+\left[\frac{k_2\exp(-k_1 t) - k_1\exp(-k_2 t)}{(k_1 - k_2)}\right]\right)$$

(S13)

$$\tau(t) = \tau_{N,0.0}\exp(-k_1 t) + \tau_{I,0.0}k_1\frac{[\exp((-k_1 t) - \exp(-k_2 t)]}{(k_2 - k_1)} + \tau_{U,0.0}\left(1+\left[\frac{k_2\exp(-k_1 t) - k_1\exp(-k_2 t)}{(k_1 - k_2)}\right]\right)$$

(S14)

Here, k_1 and k_2 are the two microscopic rate constants shown in model 2, $F_{I,0.0}$ and $\tau_{I,0.0}$ are the relative fluorescence intensity and mean lifetime, respectively, for the intermediate, I, in the absence of quencher.

In the presence of 0.6 M quencher, the unfolding kinetic traces are described by Eqs. S15 (fluorescence intensity data) and S16 (fluorescence lifetime data):

$$F(t) = F_{N,0.6}\exp(-k_1 t) + F_{I,0.6}k_1\frac{[\exp((-k_1 t) - \exp(-k_2 t)]}{(k_2 - k_1)} + F_{U,0.6}\left(1+\left[\frac{k_2\exp(-k_1 t) - k_1\exp(-k_2 t)}{(k_1 - k_2)}\right]\right)$$

(S15)

$$\tau(t) = \tau_{N,0.6}\exp(-k_1 t) + \tau_{I,0.6}k_1\frac{[\exp((-k_1 t) - \exp(-k_2 t)]}{(k_2 - k_1)} + \tau_{U,0.6}\left(1+\left[\frac{k_2\exp(-k_1 t) - k_1\exp(-k_2 t)}{(k_1 - k_2)}\right]\right)$$

(S16)

$F_{I,0.6}$ and $\tau_{I,0.6}$ are the relative fluorescence intensity and mean lifetime, respectively for the intermediate, I, in the presence of 0.6 M quencher.

To fit the kinetic traces for unfolding in the absence and presence of 0.6 M quencher, the kinetic trace in the presence of quencher was first fit to Eqs. S15 and S16 to obtain the values of k_1, k_2 and $F_{I,0.6}$ (or $\tau_{I,0.6}$). Then, the kinetic trace obtained in the absence of quencher was fit to Eqs. S13 and S14, constraining the values of k_1 and k_2 to those already obtained, to obtain the value of $F_{I,0.0}$ (or $\tau_{I,0.0}$).

For three-state unfolding, the value of k_q (t) at each time t, is given by Eq. S17:

$$k_q(t) = \frac{\left[\frac{\tau_{0.0}(t)}{\tau_{0.6}(t)} - 1\right]}{0.6\ \tau_{a,0.0}(t)} \quad \text{(S17)}$$

where $\tau_{0.0}$ (t) is given by Eq. S18, and $\tau_{0.6}$ (t) is given by Eq. S16. It should be noted that fitting the time evolution of τ_m data in the absence of quencher to the three-state model gives the τ_m value of I_L as a single quantity (individual components cannot be obtained) and so τ_a cannot be calculated for I_L. Hence, τ_m is used for the calculation of k_q of I_L. However, the order of magnitude of k_q for the N or the U state did not differ, irrespective of the lifetime used.

Fitting equilibrium and kinetic data monitored by fluorescence and CD

Equilibrium unfolding data monitored by fluorescence and CD were fitted according to a two-state N↔U model, to determine the free energy change of unfolding [$\Delta G_U(H_2O)$] and the mid-point of transition (C_M) (1).

Kinetic traces monitored by CD and fluorescence signals were fitted with either of the equations given by,

$$S(t) = S_\infty + S_a \exp(-k_1 t) \quad \text{(S18)}$$

$$S(t) = S_\infty + S_a \exp(-k_1 t) + S_b \exp(-k_2 t) \quad \text{(S19)}$$

where S(t), S_∞, S_a and S_b are the signals at time t, at the completion of the unfolding process, and the amplitudes of the phases having the rate constants k_1 and k_2 respectively.

Global fitting of the kinetic data

Unfolding kinetic traces obtained from the use of multiple probes were fitted globally using MATLAB. The traces were simulated using the function *ode23s* which requires an initial set of values for all the fitting parameters such as the microscopic rate constants and the optical properties of the intermediates. In the analysis, successive iterations were carried out by varying the fitting parameters, and the function *fminsearch* was used to search for the fit which has the lowest value of root-mean-square difference between the experimental and simulated traces. All the steps of the multi-step mechanism were kept reversible. In the fitting, the values of microscopic rate constants for the forward and backward steps were varied under the constraint that the overall equilibrium constant of unfolding was the same as obtained from the equilibrium unfolding experiment. The forward and backward rates of the first step in the multi-step mechanism was constrained to be greater than 1000 s^{-1} in the fitting in order to represent the burst phase signal changes as observed in the near-UV CD and fluorescence data.

Supporting Material References:

1. Sridevi, K., and J. B. Udgaonkar. 2003. Surface Expansion Is Independent of and Occurs Faster than Core Solvation during the Unfolding of Barstar. Biochemistry 42:1551-1563.

2. Sinha, K. K., and J. B. Udgaonkar. 2007. Dissecting the non-specific and specific components of the initial folding reaction of barstar by multi-site FRET measurements. J. Mol. Biol. 370:385–405.
3. Jha, S. K., D. Dhar, G. Krishnamoorthy, and J. B. Udgaonkar. 2009 Continuous dissolution of structure during the unfolding of a small protein. Proc. Natl. Acad. Sci. USA 106:11113-11118.
4. Jha, S. K., and J. B. Udgaonkar. 2009. Direct evidence for a dry molten globule intermediate during the unfolding of a small protein. Proc. Natl. Acad. Sci. USA 106:12289-12294.
5. Lakowicz, J. R., B. Maliwal, H. Cherek, and A. Balter. 1983. Rotational freedom of tryptophan residues in proteins and peptides. Biochemistry 22:1741-1752.
6. Barshop, B. A., R. F. Wrenn, and C. Frieden. 1983. Analysis of numerical methods for computer simulation of kinetic processes: Development of KINSIM--A flexible, portable system. Anal. Biochem. 130:134-145.

Supporting Material Figure legends:

FIGURE S1. Kinetic curves of unfolding of unlabeled and TNB-labeled proteins. Far-UV CD at 222 nm was used to monitor the unfolding of Cys82 (panel A), Cys82-TNB (panel B), Cys25 (panel C) and Cys25-TNB (panel D) in 5.5 M urea at 10 ^{o}C. The solid black lines through the data are exponential fits which yield the rates of 0.30, 0.29, 0.34 and 0.37 s^{-1} for the data in the panels A, B, C and D respectively.

FIGURE S2. Quenching of W53 fluorescence by KI. (A) Stern-Volmer plots for W53 quenching in the N (inverted triangles) and U states (triangles). The mean fluorescence lifetime of W53 was measured in absence (τ_0) and in presence of KI (τ), and τ_0/τ is plotted as a function of KI concentration. The solid line through the data is a fit to a linear equation with intercept of 1 and the slope is the Stern-Volmer constant (K_{SV}) from which the k_q values were calculated (see Materials and Methods). (B and C) Unfolding kinetics of barstar in 5.5 M urea and 10 ^{o}C was monitored by measurement of the changes in the τ_m of W53 during unfolding in the presence of 0.6 M KCl (o) and 0.6 M KI (o) (panel B). The kinetic traces have been normalized to between values of 1 for completely native protein and 0 for completely unfolded protein (panel C). The dashed black lines through the data are fits to a N $\rightarrow$ I_L $\rightarrow$ U model (Eqs. S14 and S16, see Materials and Methods of Supporting Material). The fits yield apparent rates for the N $\rightarrow$ I and I $\rightarrow$ U steps of 0.72 s^{-1} and 0.32 s^{-1}, respectively. The mean lifetimes for N, I_L and U obtained from the fits were 4.00, 1.30, 1.10 ns, respectively, in the presence of 0.6 M KI, and 4.31, 3.90. 3.40 ns, respectively in the presence of 0.6 M KCl (panel B). (D) Unfolding kinetics of barstar monitored by fluorescence intensity measurement at 350 nm. Kinetic traces of the unfolding of barstar in the presence of 0.6 M KCl (solid cyan line) and of 0.6 M KI (solid brown line) are shown. Each kinetic trace is normalized to the native signal of 1 in the presence of 0.6 M KCl. The solid black lines through the data are fits to the three-state N $\rightarrow$ I_L $\rightarrow$ U model. The fits yield apparent rates for the N $\rightarrow$ I_L and I_L $\rightarrow$ U steps of 0.71 and 0.31 s^{-1}, respectively (see Materials and Methods of Supporting Material). The fluorescence intensities for N, I_L and U used in the obtained from the fits were 0.95, 0.78 and 0.58 ns, respectively, in the presence of 0.6 M KCl, and 0.87, 0.20, 0.16 ns, respectively, in the presence of 0.6 M KI. (E and F) Evolution of Stern-Volmer constant (K_{SV}) and bimolecular fluorescence quenching constant (k_q) during unfolding. K_{SV} (panel E) and k_q (panel F) values (Δ) were calculated at each time point during unfolding from the τ_m values (see Materials and Methods of Supporting Material), and are plotted as function of unfolding time. The black dashed line through the data is a simulated fit (see Materials and Methods of Supporting Material) to the N $\rightarrow$ I_L $\rightarrow$ U model, using parameter values from the fits to the data in panel B. The dashed blue line represents the value for the N state.

FIGURE S3. Fluorescence anisotropy decays at different times of unfolding 0.5 M urea at 10 ^{o}C. Representative fluorescence anisotropy decay curves at 0.26 s (A), 0.46 s (B), 2.06 s (C) and 5.06 s (D) are shown. The solid black lines through the data represent fits to a two-exponential equation. In each panel, the upper *inset* shows the residuals from fitting the data to a single exponential equation, and the bottom *inset* shows the residuals from fitting the data to a two-exponential equation.

FIGURE S4. Kinetic simulations to the five-state N $\rightarrow$ N* $\rightarrow$ I_E $\rightarrow$ I_L $\rightarrow$ U mechanism. Panels A-F show kinetic simulations to a five-state model along with the experimental time courses of the observed change in fluorescence in the absence of acrylamide, the observed change in fluorescence in the presence of 0.6 M acrylamide, the far-UV CD signal change,

the change in near-UV CD signal, the fluorescence signal change for Cys25-TNB and the change in the value of β_{local}, respectively. In panels A-E, the solid lines show the experimentally determined kinetic curves whereas the triangles show the time evolution of β_{local} in panel F. The dotted line in each panel represents the simulated data which starts from either the native signal or from a value obtained from the extrapolation of native baseline of equilibrium measurement. Each panel shows the mechanism and rate constants used, along with the optical properties of N (F_N), N* (F_{N*}), I_E (F_{IE}) I_L (F_{IL}) and U (F_U) used to generate the simulated kinetic curves obtained from the kinetic simulations carried out using the program KINSIM (6). In the simulations, the rate constants used for the $N^* \rightarrow I_E$, $I_E \rightarrow I_L$ and $I_L \rightarrow U$ steps were those observed in the FRET measurements, time-resolved anisotropy decay measurements, and the fluorescence quenching experiment.

FIGURE S5. Global fitting of the data to the five-state $N \leftrightarrow N^* \leftrightarrow I_E \leftrightarrow I_L \leftrightarrow U$ mechanism. Panels A-F show fit to a five-state model along with the experimentally determined time courses of the observed change in fluorescence in the absence of acrylamide, the observed change in fluorescence in the presence of 0.6 M acrylamide, the far-UV CD signal change, the change in near-UV CD signal, the fluorescence signal change for Cys25-TNB, and the change in the value of β_{local}, respectively. In panels A-E, the solid lines show the experimentally determined kinetic curves whereas the triangles show the time evolution of experimental value of β_{local} in panel F. The dotted line in each panel represents the fit which starts from either the native signal or from a value obtained from the extrapolation of native baseline (i.e. from the dependence of native protein baseline on the concentration of denaturant obtained from equilibrium measurements). Each panel shows the mechanism and rate constants along with the optical properties of N (F_N), N* (F_{N*}), I_E (F_{IE}) I_L (F_{IL}) and U (F_U) obtained from the fitting of the data using the MATLAB program. The forward rate constant for any of the steps in this reversible model differs with the corresponding rate constant of the irreversible model used in the kinetic simulations as expected from kinetic models (see Figure legend of Fig. S4).

FIGURE S6. Global fitting of the data to a four-state $N \leftrightarrow I_1 \leftrightarrow I_2 \leftrightarrow U$ mechanism. Panels A-F show fits to a four-state model along with the experimentally determined time courses of the observed change in fluorescence in the absence of acrylamide, the observed change in fluorescence in the presence of 0.6 M acrylamide, the far-UV CD signal change, the change in near-UV CD signal, the fluorescence signal change for Cys25-TNB, and the change in the value of β_{local}, respectively. In panels A-E, the solid lines show the experimentally determined kinetic curves whereas the triangles show the time evolution of experimental value of β_{local} in panel F. The dotted line in each panel represents the fit which starts from either the native signal or from a value obtained from the extrapolation of native protein baseline of an equilibrium unfolding curve. Each panel shows the mechanism and rate constants along with the optical properties of N (F_N), I_1 (F_{I1}), I_2 (F_{I2}) and U (F_U) obtained from the fitting of the data using MATLAB program.

FIGURE S7. Comparison of residuals from the fitting of the data to a five-state $N \leftrightarrow N^* \leftrightarrow I_E \leftrightarrow I_L \leftrightarrow U$ mechanism, and to a four-state $N \leftrightarrow I_1 \leftrightarrow I_2 \leftrightarrow U$ mechanism. Panels A, C, E, G, I and K show the residuals for the global fitting of the data to five-state model (Figure S5) whereas panels B, D, F, H, J and L show the residuals for the global fitting of the data to the four-state model (Figure S6). The residuals from the fits to the kinetic traces for the observed change in fluorescence in the absence of acrylamide (panels A and B), the observed change in fluorescence in the presence of 0.6 M acrylamide (panels C and D), the far-UV CD signal change (panels E and F), the change in near-UV CD signal (panels G and H), the

fluorescence signal change for Cys25-TNB (panels I and J), and the change in the value of β_{local} (panels K and L) are shown.

FIGURE S8. Global fitting of the all the data except the Cys25-TNB data to the four-state N $\leftrightarrow$ I_A $\leftrightarrow$ I_B $\leftrightarrow$ U mechanism. Panels A-E show fits to a four-state model along with the experimentally determined time courses of the observed change in fluorescence in the absence of acrylamide, the observed change in fluorescence in the presence of 0.6 M acrylamide, the far-UV CD signal change, the change in near-UV CD signal and the change in the value of β_{local}, respectively. In panels A-D, the solid lines show the experimentally determined kinetic curves whereas triangles show the time evolution of experimental value of β_{local} in panel E. The dotted line in each panel represents the fit which starts from either the native signal or from a value obtained from the extrapolation of the native protein baseline of an equilibrium unfolding curve. Each panel shows the mechanism and rate constants along with the optical properties of N (F_N), I_A (F_{IA}), I_B (F_{IB}) and U (F_U) obtained from the fitting of the data using MATLAB program.

FIGURE S9. Global fitting of the all the data except the Cys25-TNB data to the three-state N $\leftrightarrow$ I $\leftrightarrow$ U mechanism. Panels A-E show fits to a three-state model along with the experimentally determined time courses of the observed change in fluorescence in the absence of acrylamide, the observed change in fluorescence in the presence of 0.6 M acrylamide, the far-UV CD signal change, the change in near-UV CD signal and the change in the value of β_{local}, respectively. In panels A-D, the solid lines show the experimentally determined kinetic curves whereas triangles show the time evolution of experimental value of β_{local} in panel E. The dotted line in each panel represents the fit which starts from either the native signal or from a value obtained from the extrapolation of the native protein baseline. Each panel shows the mechanism and rate constants along with the optical properties of N (F_N), I (F_I) and U (F_U) obtained from the fitting of the data using MATLAB program.

FIGURE S10. Comparison of residuals from the fitting of all the data except the Cys25-TNB data to a four-state N $\leftrightarrow$ I_A $\leftrightarrow$ I_B $\leftrightarrow$ U mechanism and to a three-state N $\leftrightarrow$ I $\leftrightarrow$ U mechanisms. Panels A, C, E, G and I show the residuals from the global fitting of the data to the four-state model (Figure S8) whereas panels B, D, F, H and J show the residuals for the global fitting of the data to three-state model (Figure S9). The residuals from the fitting of the kinetic traces for the observed change in fluorescence in the absence of acrylamide (panels A and B), the observed change in fluorescence in the presence of 0.6 M acrylamide (panels C and D), the far-UV CD signal change (panels E and F), the change in near-UV CD signal (panels G and H) and the change in the value of β_{local} (panels I and J) are shown.

Supporting Material Figures

FIGURE S1

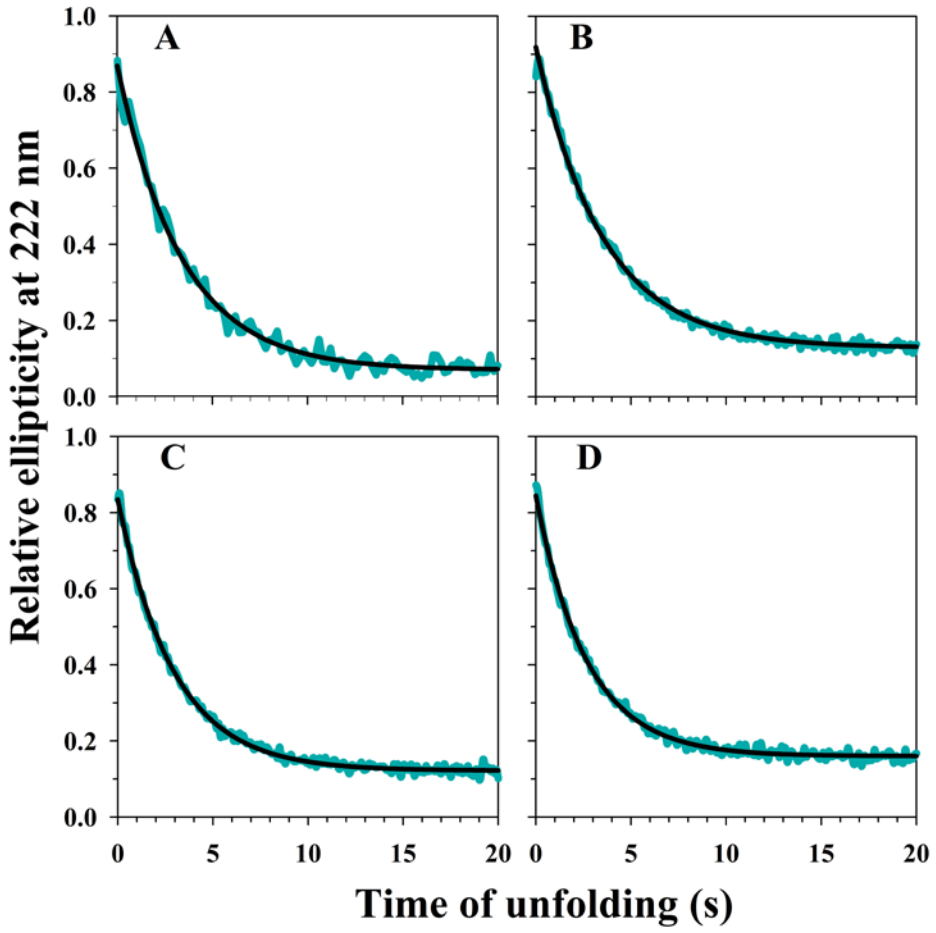

FIGURE S2

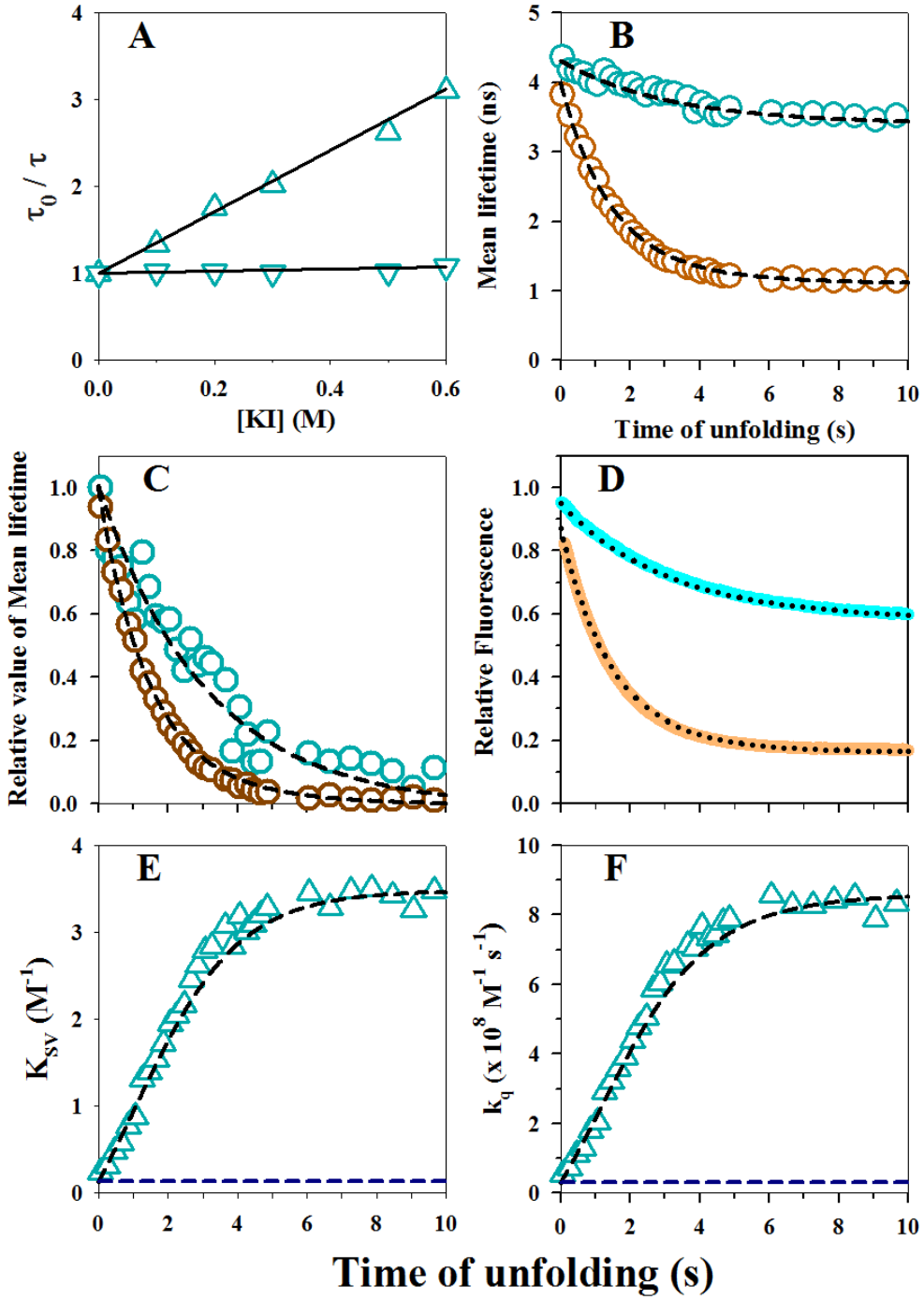
A
B
C
D
E
F
τ_0 / τ
[KI] (M)
Mean lifetime (ns)
Time of unfolding (s)
Relative value of Mean lifetime
Relative Fluorescence
K_{SV} (M^{-1})
k_q (x 10^8 M^{-1} s^{-1})
Time of unfolding (s)

FIGURE S3

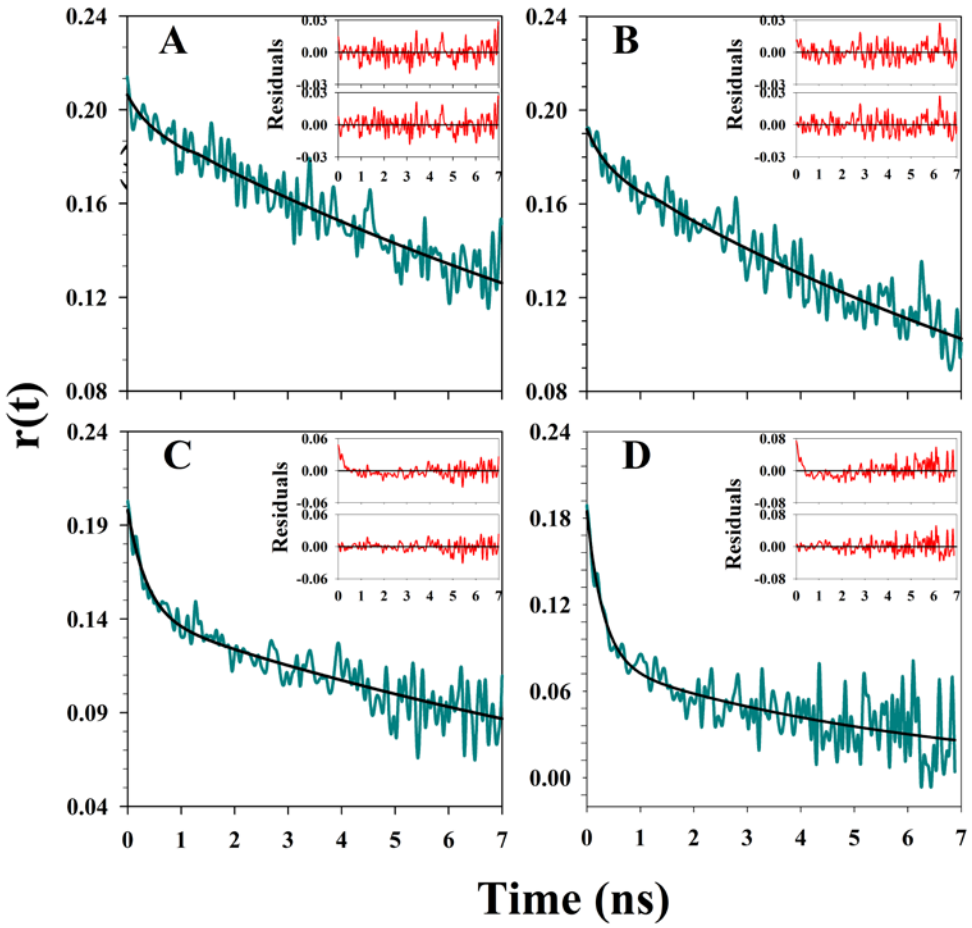

FIGURE S4

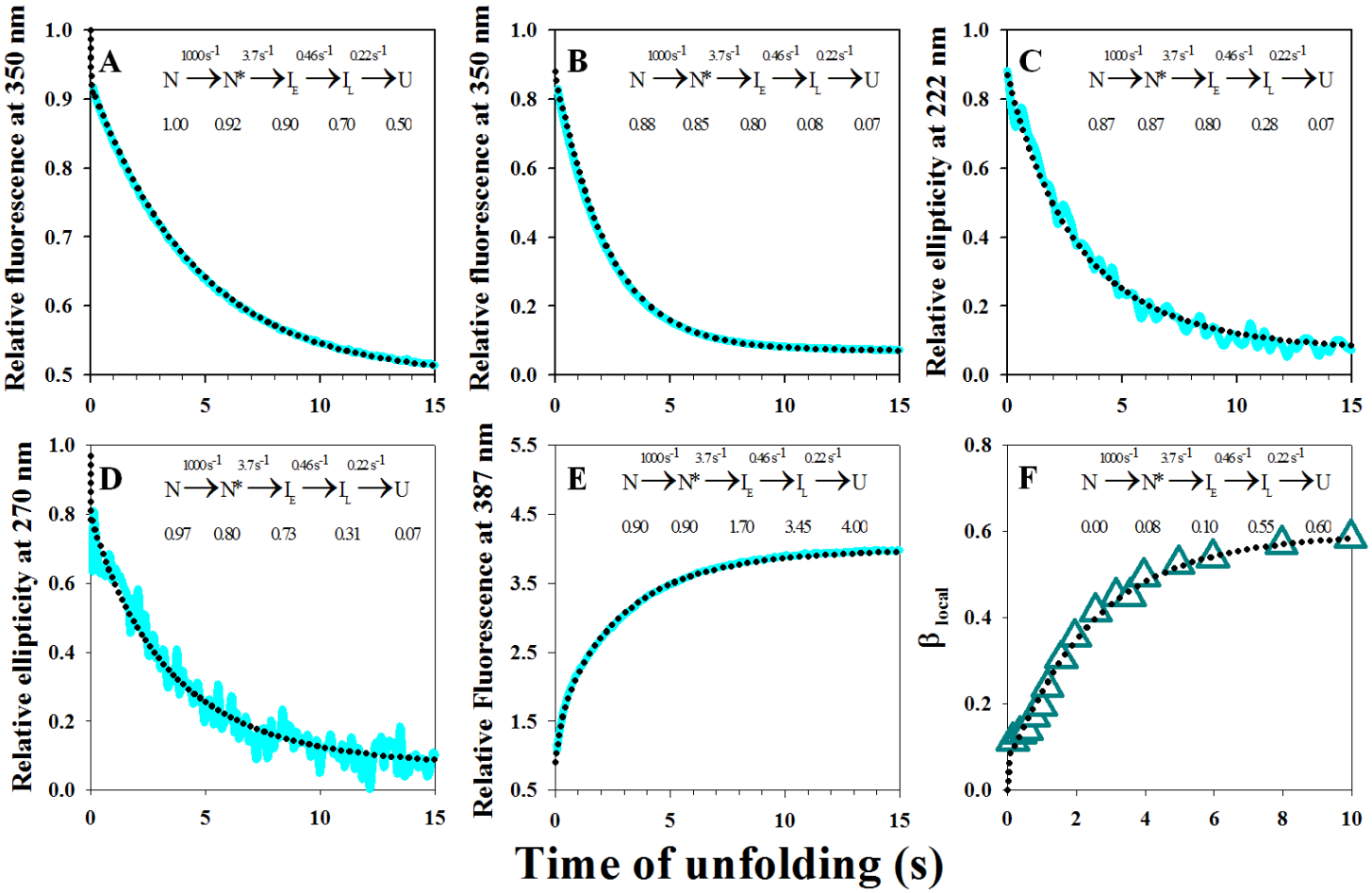
A
B
C
D
E
F
N → N* → I_E → I_L → U
1000 s-1 3.7 s-1 0.46 s-1 0.22 s-1
1.00 0.92 0.90 0.70 0.50
0.88 0.85 0.80 0.08 0.07
0.87 0.87 0.80 0.28 0.07
0.97 0.80 0.73 0.31 0.07
0.90 0.90 1.70 3.45 4.00
0.00 0.08 0.10 0.55 0.60
Relative fluorescence at 350 nm
Relative ellipticity at 222 nm
Relative ellipticity at 270 nm
Relative Fluorescence at 387 nm
β local
Time of unfolding (s)

FIGURE S5

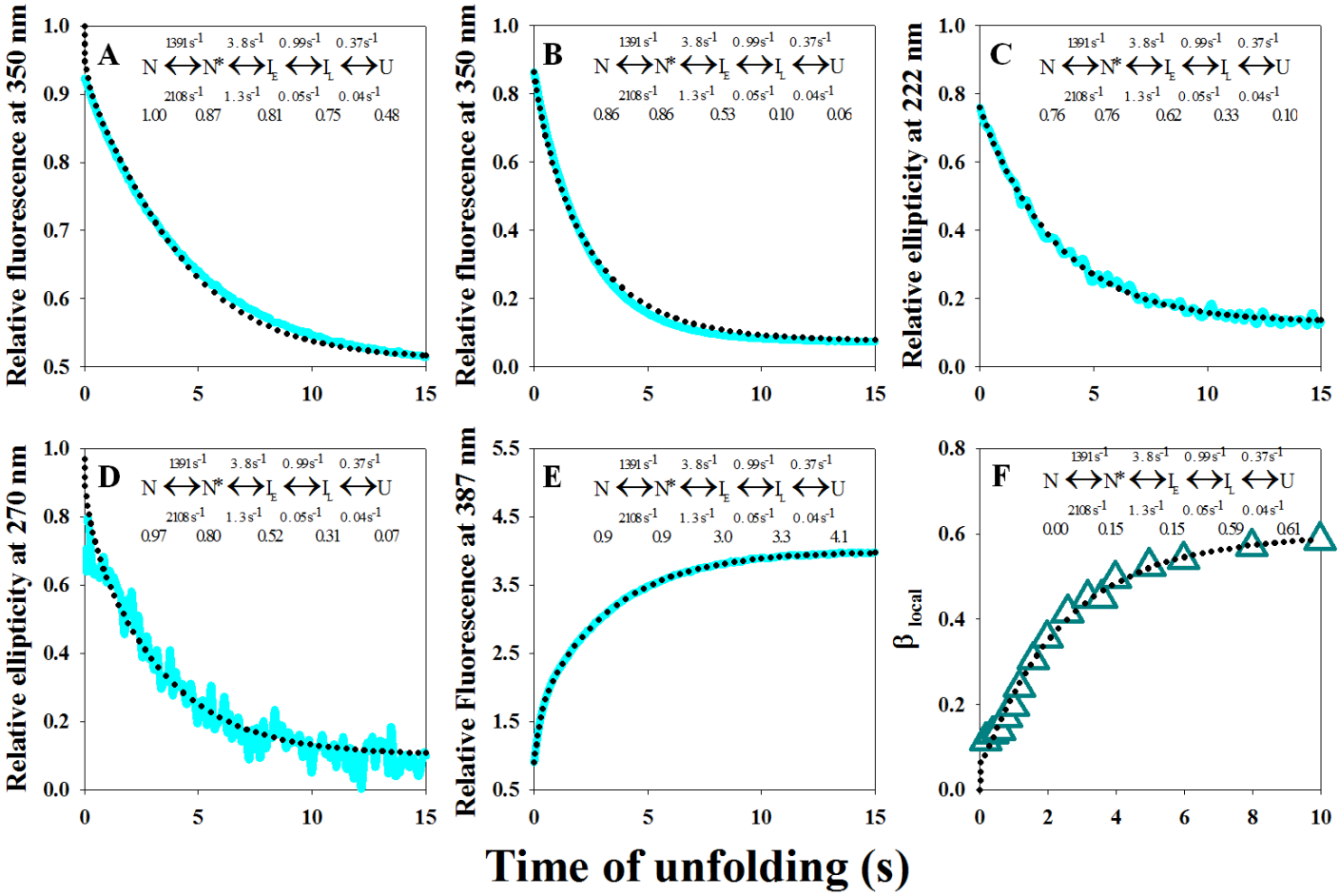
A
B
C
D
E
F
N ↔ N* ↔ I_E ↔ I_L ↔ U
1391 s-1 3.8 s-1 0.99 s-1 0.37 s-1
2108 s-1 1.3 s-1 0.05 s-1 0.04 s-1
1.00 0.87 0.81 0.75 0.48
0.86 0.86 0.53 0.10 0.06
0.76 0.76 0.62 0.33 0.10
0.97 0.80 0.52 0.31 0.07
0.9 0.9 3.0 3.3 4.1
0.00 0.15 0.15 0.59 0.61
Relative fluorescence at 350 nm
Relative ellipticity at 222 nm
Relative ellipticity at 270 nm
Relative Fluorescence at 387 nm
β local
Time of unfolding (s)

FIGURE S6

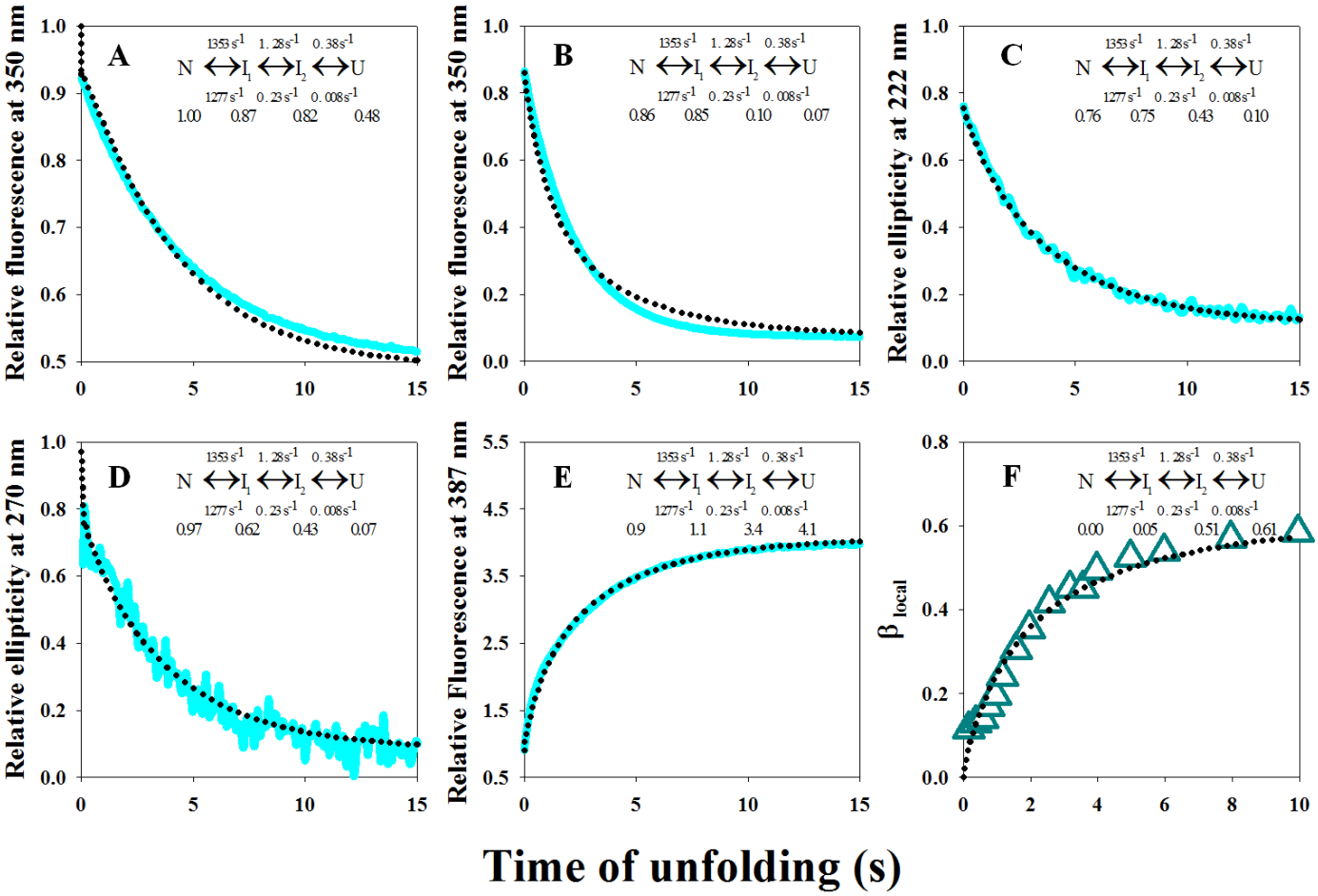
A
B
C
D
E
F
N ↔ I1 ↔ I2 ↔ U
1353 s-1 1.28 s-1 0.38 s-1
1277 s-1 0.23 s-1 0.008 s-1
1.00 0.87 0.82 0.48
0.86 0.85 0.10 0.07
0.76 0.75 0.43 0.10
0.97 0.62 0.43 0.07
0.9 1.1 3.4 4.1
0.00 0.05 0.51 0.61
Relative fluorescence at 350 nm
Relative ellipticity at 222 nm
Relative ellipticity at 270 nm
Relative Fluorescence at 387 nm
βlocal
Time of unfolding (s)

FIGURE S7

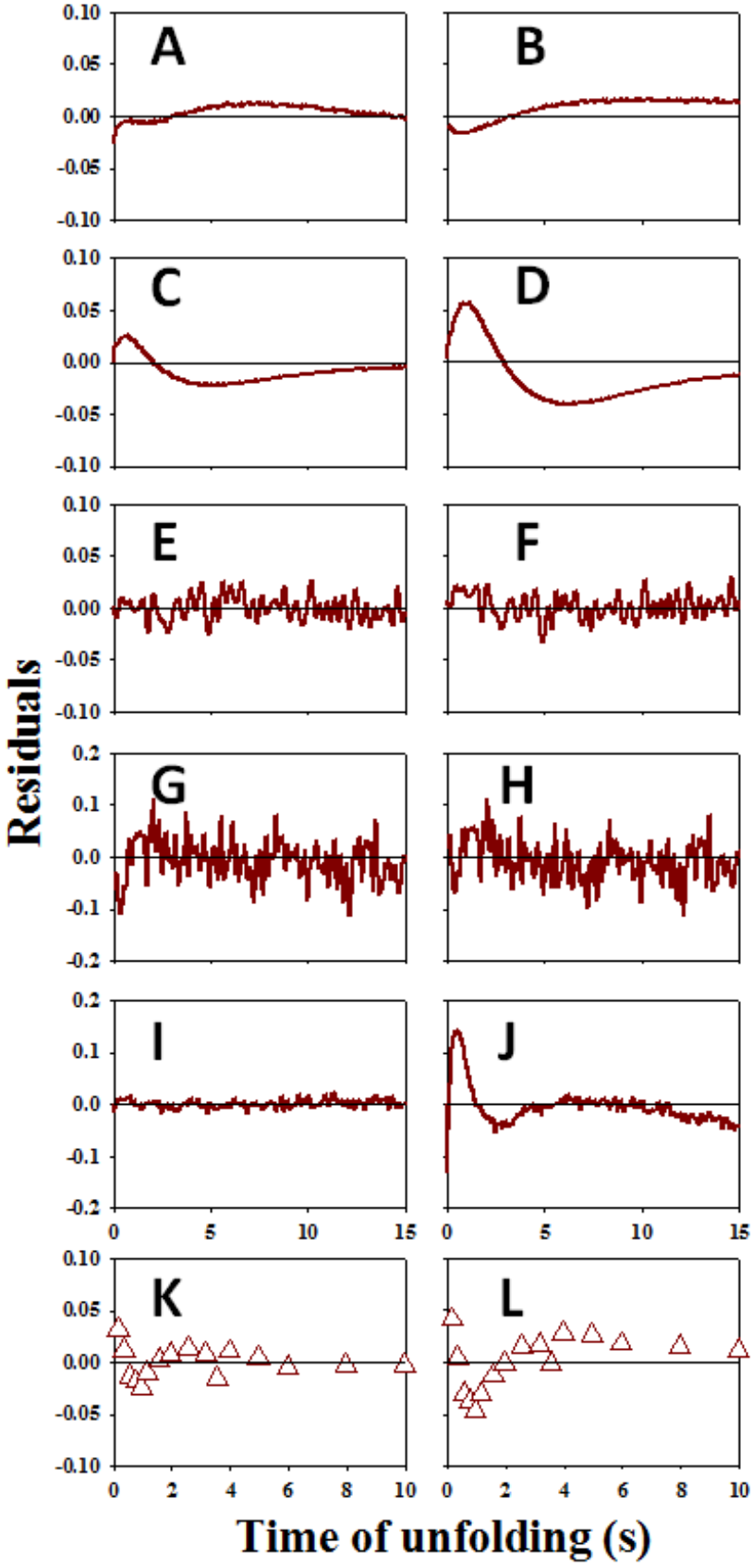

FIGURE S8

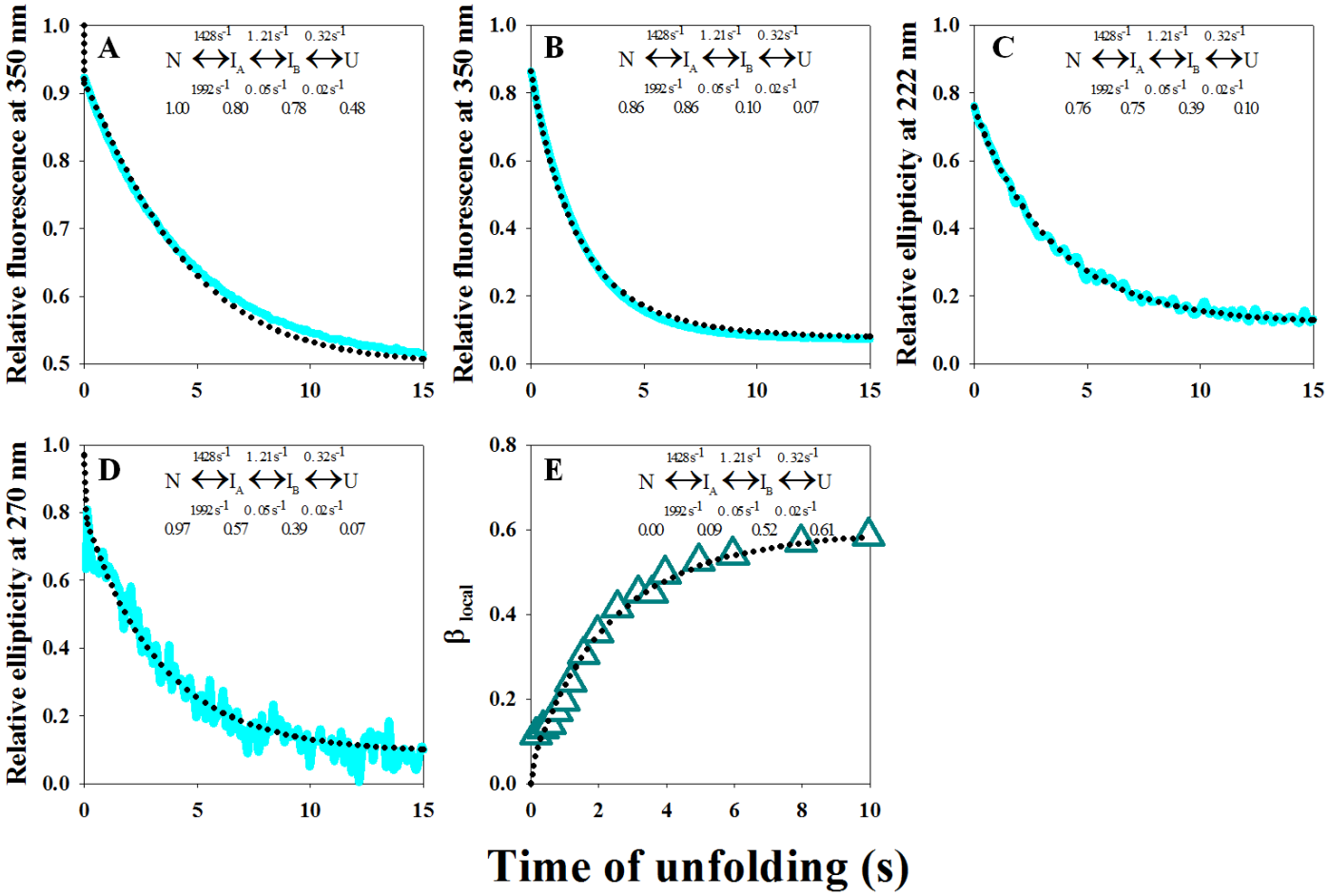
A
B
C
D
E
N ↔ I_A ↔ I_B ↔ U
1428 s^-1 1.21 s^-1 0.32 s^-1
1992 s^-1 0.05 s^-1 0.02 s^-1
1.00 0.80 0.78 0.48
0.86 0.86 0.10 0.07
0.76 0.75 0.39 0.10
0.97 0.57 0.39 0.07
0.00 0.09 0.52 0.61
Relative fluorescence at 350 nm
Relative ellipticity at 222 nm
Relative ellipticity at 270 nm
β local
Time of unfolding (s)

FIGURE S9

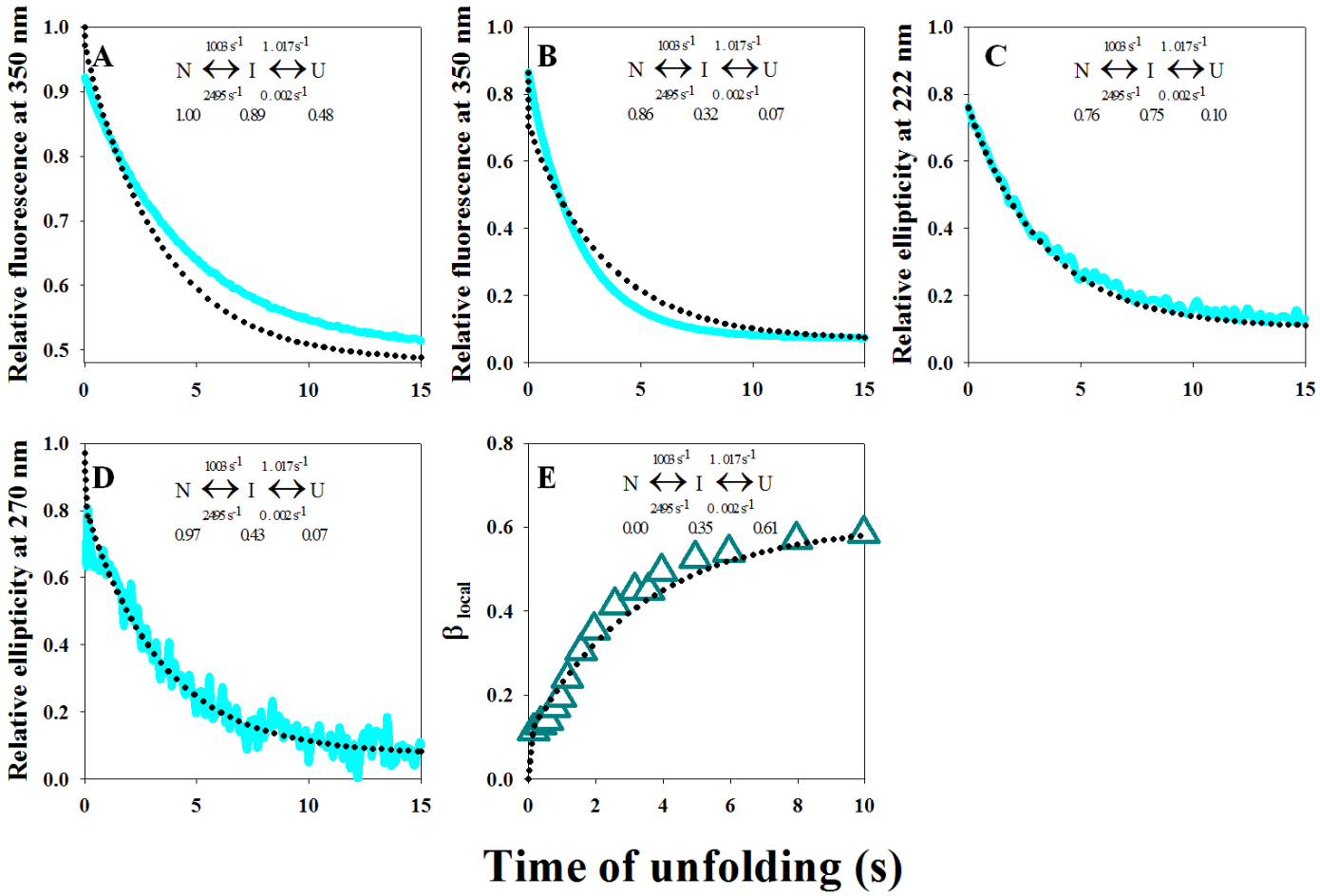
A
B
C
D
E
N ↔ I ↔ U
1.00 0.89 0.48
0.86 0.32 0.07
0.76 0.75 0.10
0.97 0.43 0.07
0.00 0.35 0.61
Relative fluorescence at 350 nm
Relative ellipticity at 222 nm
Relative ellipticity at 270 nm
β local
Time of unfolding (s)

FIGURE S10